Available online at www.sciencedirect.com
ScienceDirect
Trans. Nonferrous Met. Soc. China 33(2023) 1086−1097
Transactions of Nonferrous Metals Society of China
www.tnmsc.cn

Effect of dual-heterogeneous microstructures on mechanical properties of AZ91 extruded sheet

Shuai-shuai LIU[1,2], Bang-peng YANG[1,2], Guang-sheng HUANG[1,2], Xian-hua CHEN[1,2], Ai-tao TANG[1,2], Bin JIANG[1,2], Kai-hong ZHENG[3], Fu-sheng PAN[1,2]

1. State Key Laboratory of Mechanical Transmission, College of Materials Science and Engineering, Chongqing University, Chongqing 400044, China;
2. National Engineering Research Center for Magnesium Alloys, Chongqing University, Chongqing 400044, China;
3. Institute of New Materials, Guangdong Academy of Sciences, Guangzhou 510650, China

Received 2 December 2021; accepted 29 March 2022

Abstract: The influence of dual-heterostructure of grain size and precipitates on the mechanical properties of the AZ91 alloy extruded sheet prepared by small extrusion ratio was investigated. Compared to the sample with the extrusion ratio (ER) of 12.8 (i.e., ER12.8 sample), the ER3.9 and ER6.4 samples present a remarkable coarse and fine-grained layers with heterogeneous fine-dispersed precipitates. Moreover, a large number of banded precipitates are observed in the fine-grained layers of the ER3.9 sample. The ER6.4 sample has an excellent combination of strength and ductility due to a balance of heterogeneous deformation-induced (HDI) stress and precipitates. Although the ER3.9 sample shows the highest HDI stress and Schmid factor for basal slip to improve ductility, more banded precipitates still play a dominate role in deteriorating its mechanical properties.

Key words: AZ91 alloy; dual-heterostructure; precipitates; mechanical properties; heterogeneous deformation-induced (HDI) stress

1 Introduction

Mg alloys, as the lightest structural metallic materials, have been widely used in building construction, automobile, power and aerospace, etc., which greatly relieve present challenge of energy crisis [1−3]. However, a few activated slip systems lead to low ductility at room temperature, restricting their engineering applications [4,5]. Therefore, it is urgent to search a feasible method to achieve outstanding combination of strength and ductility of Mg alloys.

Recently, WU et al [6] prepared the pure Ti with heterogeneous lamella structure, which was composed of deformed coarse grains and recrystallized ultrafine grains. Mechanical tests indicated that it exhibited a strength comparable to ultrafine-grained metals and ductility similar to that of conventional coarse-grained metals, evading the conventional trade-off between strength and ductility. Some similar studies with hetero-structures, such as IF steel [7], Ni/Cu/Ni [8] and Cu−Cu10Zn, [9] display excellent strength−ductility synergy. Among these materials, the soft and hard domains have dramatic differences in flow stress. The geometrically necessary dislocations (GNDs) will accumulate at the domain interface of soft domain to accommodate the strain gradient during deformation [10,11]. The increasing strain gradient at the domain interface generates more GNDs due to the larger strain partitioning, which

Corresponding author: Guang-sheng HUANG, Tel: +86-13635430782, E-mail: gshuang@cqu.edu.cn;
Bin JIANG, Tel: +86-13594190166, E-mail: jiangbinrong@cqu.edu.cn
DOI: 10.1016/S1003-6326(23)66167-9

induces extra heterogeneous deformation-induced (HDI) stress (previously referred to as back stress) strengthening and hardening, in addition to conventional dislocation hardening [12].

Metal materials with heterostructures can greatly alleviate traditional inversion relationship of strength−ductility dilemma. Most of researches were only focused on the design of heterogeneous grain size. Generally, the heterogeneities of metal materials include the chemical composition, texture, hardness and precipitate, etc [10]. It has been reported that dual-heterostructure metal materials can yield a good combination of strength and ductility by regulating the component heterogeneity, such as Mg−1Gd/Mg−13Gd (wt.%) alloy with the dual-heterostructure of grain size and texture [13], the brass with the heterogeneous lamella and gradient structure [14], the low carbon martensitic steel with the dual-phase heterostructure of martensite and ferrite [15]. However, the influence of dual-heterostructure of grain size and precipitates on mechanical properties has been rarely studied in previous researches. In this work, following the principle of low cost and simple preparation process, the AZ91 alloy with dual-heterostructure of grain size and precipitates was successfully prepared by small extrusion ratio (ER) due to its intense precipitation potential. The effects of dual-heterostructure on mechanical properties of AZ91 extruded sheet were discussed in detail. The mechanisms with excellent strength−ductility synergy were systematically illustrated.

2 Experimental

In the present study, the AZ91 (Mg−9.06Al−0.59Zn, wt.%) ingots were initially cut into the cuboid blocks with the dimension of 15 mm × 15 mm × 35 mm. As shown in Fig. 1, these cuboid blocks were solid-solution (SS) treated at 420 °C for 20 h and quenched in water immediately. After that, the treated cuboid blocks were extruded into sheets with the thickness of 1.5, 3 and 5 mm (normal direction, ND) by the square extrusion cylinder dies at 280 °C [16]. The corresponding ERs were 12.8, 6.4 and 3.9, which were denoted as ER12.8, ER6.4 and ER3.9 samples, respectively.

The characterizations of microstructures and texture of ER12.8, ER6.4 and ER3.9 samples were performed by the optical microscopy (OM) and field-emission scanning electron microscope (SEM, JOEL JSM 7800F) equipped with an HKL electron backscatter diffraction (EBSD) detector. The ER6.4 sample under 6.8% strain was cut into the transmission electron microscope (TEM, FEI TECNAI G2 F20) thin foils with 0.5 mm in thickness. It was ground and polished to ~50 nm in thickness, and then perforated by Ar ion milling. The tension samples were dog-bone shaped with the gauge dimension of 18 mm (extrusion direction, ED) × 4 mm (transverse direction, TD). Both uniaxial tension and loading−unloading−reloading (LUR) tests were carried out on a universal testing machine along ED with a strain rate of 1×10^{-3} s^{-1} at room temperature. During LUR tests with program control mode, the sample was loaded to a set displacement value under a rate of 0.75 mm/min, unloaded, and then reloaded to 20 N under the same conditions. To ensure the mechanical data reliability, the tensile tests and LUR tests for each sample were repeated three times. The micro-hardness tests with a 200 g load for 10 s were performed by the UHVSY-1000ZB Vickers hardness tester.

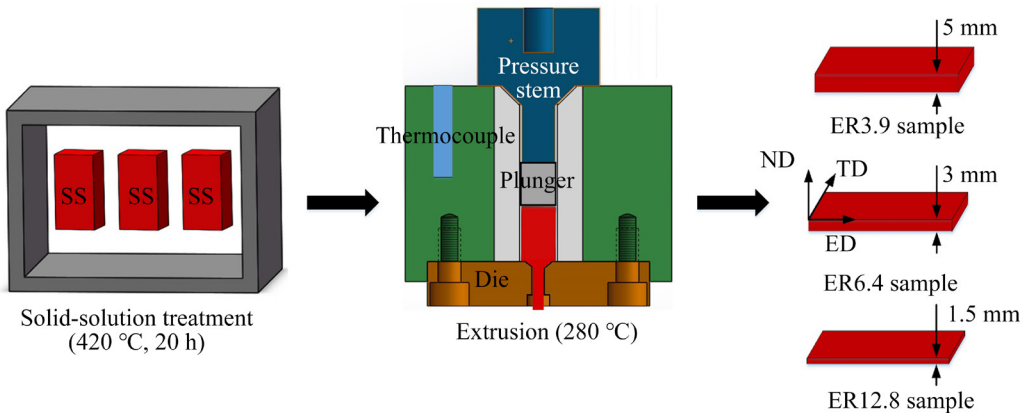

Fig. 1 Extrusion process of samples at different ERs

3 Results

3.1 Mechanical property

Figures 2(a, b) show the true stress−true strain curves and the variations in tensile properties of the samples at different ERs, respectively. It can be seen that both the ultimate tensile strength (UTS) and uniform elongation (UE) of the samples increase first and then decrease with increasing ERs, while the yield strength (YS) shows a slight downward trend. As given in Table 1, the ER6.4 sample has an outstanding combination of YS (181.3 MPa), UTS (400.5 MPa) and UE (18.3%) as compared with the ER3.9 and ER12.8 samples. It should be noted that the tensile curves of the ER6.4 and ER12.8 samples present a serrated flow. This behavior is mainly attributed to the dynamic interaction between the mobile dislocation momentarily arrested at forest dislocations and the Al and Zn solute atoms [17], which has also been studied in the Mg–8.0Al–0.7Zn–0.2Mn (wt.%) alloy [18]. However, the serrated flow behavior in the ER3.9 sample does not appear, which may be due to the generation of abundant banded $Mg_{17}Al_{12}$ precipitates, resulting in the decrease of Al solute atoms and the weakening of pinning effect.

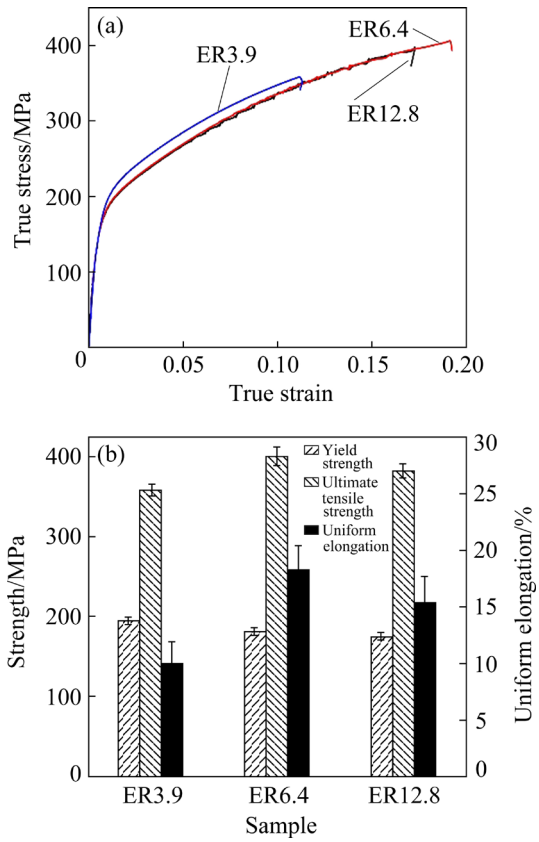

Fig. 2 True stress−strain curves of ER12.8, ER6.4 and ER3.9 samples (a), and corresponding variation trend of tensile properties (b)

Table 1 Tensile properties of samples at different ERs

Sample	YS/MPa	UTS/MPa	UE/%
ER3.9	194.8±4.2	341.3±7.5	10.0±1.9
ER6.4	181.3±4.7	400.5±11.8	18.3±2.1
ER12.8	174.0±5.1	382.2±8.9	15.4±2.3

3.2 Microstructure

Figures 3(a, b) present the typical dendritic structure of cast AZ91 alloy before SS treatment, which is identified as the γ-$Mg_{17}Al_{12}$ by energy dispersive spectrometer (EDS), as shown in Figs. 3(e, f). This finding is consistent with the previously reported results by YUAN et al [19]. After SS treatment, most of precipitates and the eutectic structure ($\alpha + \gamma$) are dissolved (Fig. 3(c)). Meanwhile, the inverse pole figure (IPF) map in Fig. 3(d) indicates that the average grain size (AGS) of the sample should be more than 500 μm and the orientation distribution is random in visible grains.

Figures 4(a−c) show the optical micrographs of the three samples on the ED−ND planes. It can be seen that the black regions of the samples gradually increase with decreasing ERs. These black regions are composed of the fine recrystallized grains and precipitates observed by the SEM micrographs. Note that significant amounts of banded $Mg_{17}Al_{12}$ precipitates, confirmed by EDS (Fig. 4(i)), are distributed in the ER3.9 sample, which leads to the initiation and propagation of cracks, deteriorating its mechanical properties. Based on the statistical results obtained by Image-Pro plus6.0 software (Figs. 4(b, c)), the area proportions of fine-grained layers in the ER3.9 and ER6.4 samples account for 32.2% and 12.7%, respectively. Therefore, the ER6.4 and ER3.9 samples exhibit a dual-heterostructure of grain and precipitates, especially the ER3.9 sample.

According to the SEM micrographs, most of precipitates are rod-like or spherical and distributed along the grain boundaries, owing to the fact that the Al atoms segregated at grain boundaries dynamically precipitate in the form of Mg−Al phase during extrusion [20]. Moreover, the amount of precipitates in the fine-grained layers is much more than that in the coarse-grained layers. On the one

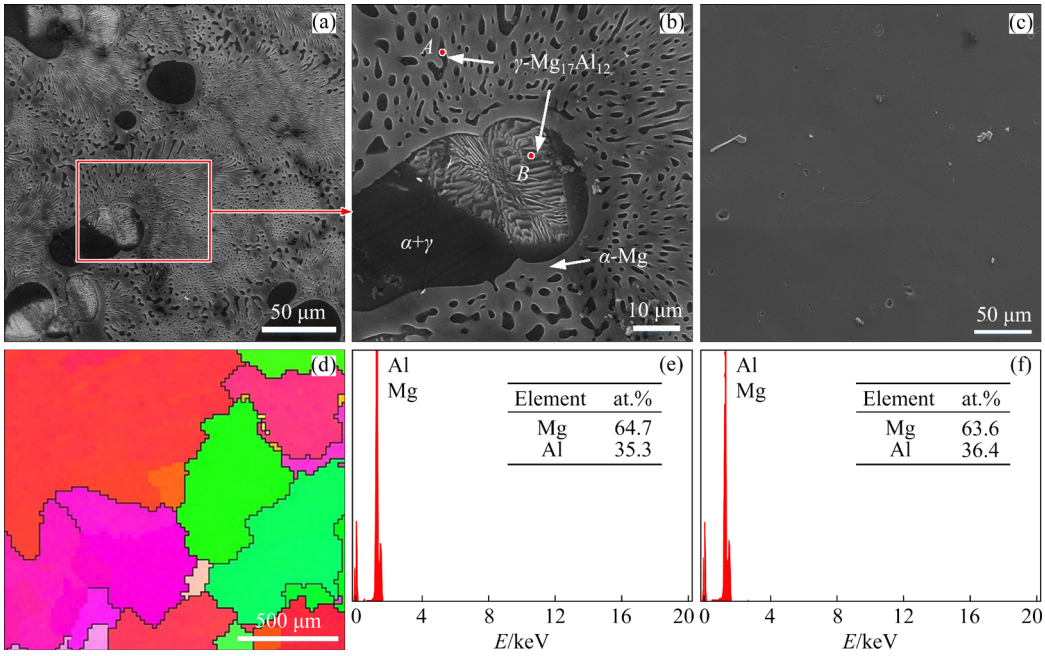

Fig. 3 SEM micrographs of sample before (a, b) and after (c) SS treatment; IPF map of sample after SS treatment (d); EDS point-scans of *A* (e) and *B* (f) marked in Fig. 3(b)

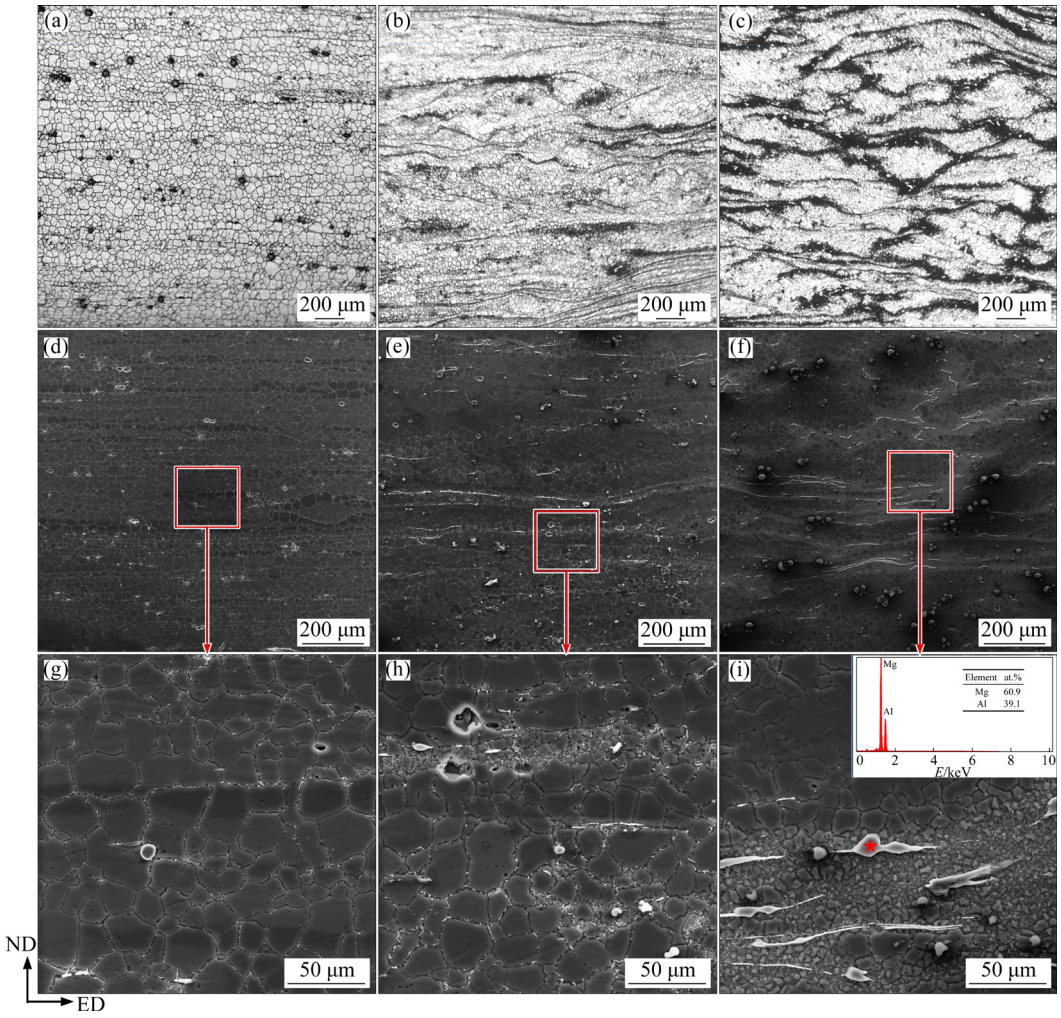

Fig. 4 Optical micrographs (a−c) and SEM micrographs (d−i) of ER12.8 (a, d, g), ER6.4 (b, e, h), and ER3.9 (c, f, i) samples

hand, the particle-stimulated nucleation (PSN) mechanism indicates that these precipitates, with a size larger than 1 μm, can provide nucleation sites for dynamic recrystallization [21−24]. On the other hand, the pinning effect of grain boundaries by precipitates inhibits the growth of dynamically recrystallized grains. Therefore, the growth rate of fine-grained layers with dense precipitates is lower than that of coarse-grained layers with precipitate-free regions, forming a dual-heterostructure of grain size and precipitates.

3.3 Fracture morphology

Figure 5 shows the fracture surfaces of samples at different ERs. As ERs decrease, the dimples size gradually reduces (Figs. 5(a−c)), which is related to the grain refinement. As shown in high-magnification SEM micrographs (Figs. 5(d, e)), some precipitates are observed in the brittle fracture zones and the bottom of dimples in the ER12.8 and ER6.4 samples. The ER12.8 sample has more brittle fracture zones than the ER6.4 sample, which is one of the reasons why the ductility of the ER6.4 sample is higher than that of the ER12.8 sample. In addition, the banded precipitates and cracks are detected in the ER3.9 sample, which is not conducive to the improvement of its ductility. The fracture behavior of the three samples is consistent with their mechanical properties.

4 Discussion

4.1 Balance of strength and ductility

Figures 6(a−c) show the IPF maps of the ER12.8, ER6.4 and ER3.9 samples, respectively. Obviously, the heterogeneous microstructure becomes more remarkable with decreasing ERs, and all samples present complete recrystallization. Meanwhile, the area proportion of fine-grained layers gradually increases. Note that the samples show some zero resolution regions owing to the existence of precipitates, especially the fine-grained layers in the ER3.9 sample. The statistical results obtained by Channel 5 software indicate that the AGS of the three samples decreases from 13.1 to 4.8 μm (Figs. 6(d−f)). This reduction in AGS, in accordance with the Hall−Petch law, is one of the reasons why the ER3.9 sample exhibits the highest YS.

As we know, the basal slip of Mg alloys possesses a low critical resolved shear stress (CRSS), which makes it easy to activate at room temperature [8,25]. The Schmid factor (SF) related

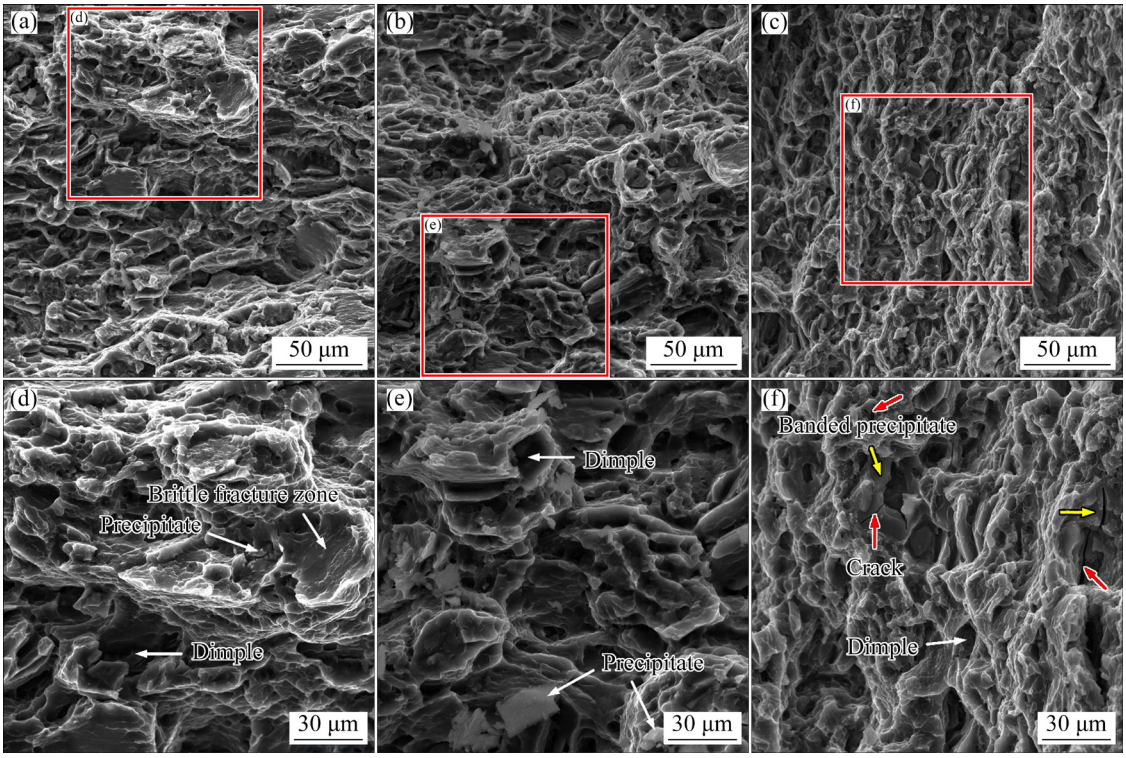

Fig. 5 SEM micrographs of fracture surfaces after tensile tests: (a, d) ER12.8 sample; (b, e) ER6.4 sample; (c, f) ER3.9 sample

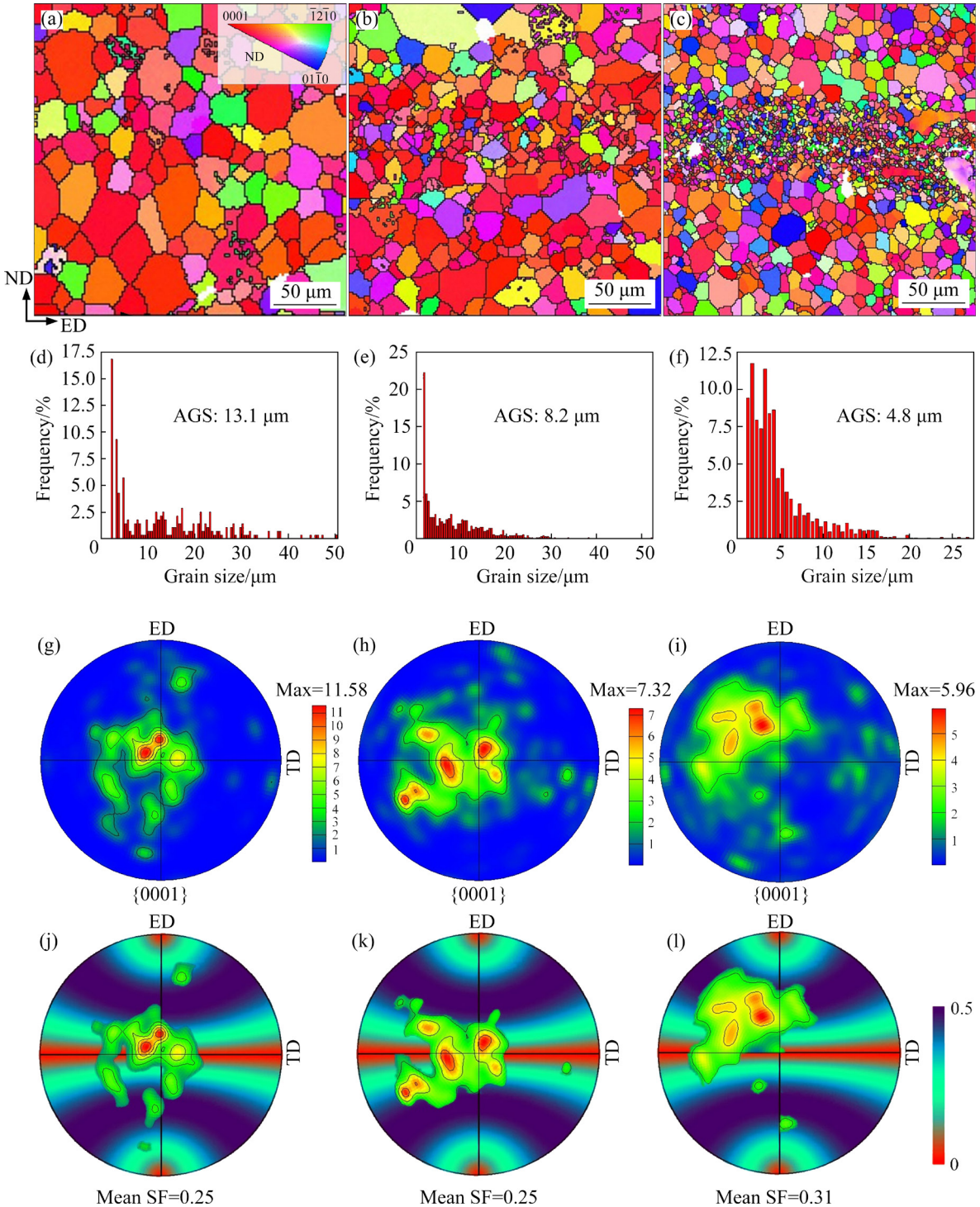

Fig. 6 IPF maps (a−c), grain size distribution (d−f), (0001) pole figures (g−i) and corresponding SF distributions in (0001) pole figures for basal slip (j−l): (a, d, g, j) ER12.8 sample; (b, e, h, k) ER6.4 sample; (c, f, i, l) ER3.9 sample

to texture plays an important role in the activation of basal slip and influences the mechanical properties of samples [24,26−28]. The (0001) pole figures of the three samples and corresponding SF distribution for basal slip on them are presented in Figs. 6(g−l). The ER12.8 and ER6.4 samples exhibit a basal texture, with their basal planes being nearly parallel to the ED. Their maximum texture intensity is mainly concentrated in the hard orientation region on the SF distribution maps (SF=0.25). Unlike the ER12.8 and ER6.4 samples, the grained *c*-axis in the ER3.9 sample are inclined by 21.7°−45.4° from the ND towards ED and TD. The majority of texture components in the ER3.9

sample are located in the soft orientation (SF=0.31), which is conducive to activating basal slip and coordinating plastic deformation when stretched along the ED. However, the ductility of the ER3.9 sample is actually lower than that of the ER6.4 and ER12.8 samples.

As illustrated in Fig. 7(a), the microhardness of the fine-grained layers in the ER3.9 sample is ~HV 82.1, which is significantly higher than that of the coarse-grained layers (~HV 61.8) due to the combined effects of grain boundaries and precipitates. The hardness value (HV 71.8) of domain interface falls between them. Thus, the coarse and fine-grained layers should exist certain extent mechanical incompatibility during heterogeneous deformation. This leads to the generation of strain gradient and induces the accumulation of GNDs at domain boundary in the coarse-grained layers to accommodate this strain gradient, inducing back stress [9,29,30]. In terms of physical process, the forward stress is formed at domain boundary in the fine-grained layers. These two stresses are collectively known as HDI stress, and they work together to produce HDI strengthening and hardening effect [15,29]. Moreover, the high density precipitates in the fine-grained layers make them harder, which exacerbates the accumulation of GNDs at domain boundary, further boosting the HDI stress [21]. The above microstructure characterization indicates that both the ER6.4 and ER3.9 samples show a dual-heterostructure of grain size and precipitates, especially the ER3.9 sample. Thus, compared with the ER6.4 and ER12.8 samples, the ER3.9 sample theoretically should exhibit higher HDI stress.

In order to quantitatively study the evolution of HDI stress after the heterogeneous deformation, the loading−unloading−reloading (LUR) tests are carried out, as shown in Fig. 7(b). Note that three samples present plump hysteresis loops at early deformation stage (Fig. 7(c)), which demonstrates the existence of a strong Bauschinger effect. The HDI stress can be calculated by Eq. (1), as derived in previous literature [31−34]:

$$\sigma_{HDI}=(\sigma_r+\sigma_u)/2 \quad (1)$$

where σ_r and σ_u represent the reloading yield stress and unloading yield stress, respectively, as

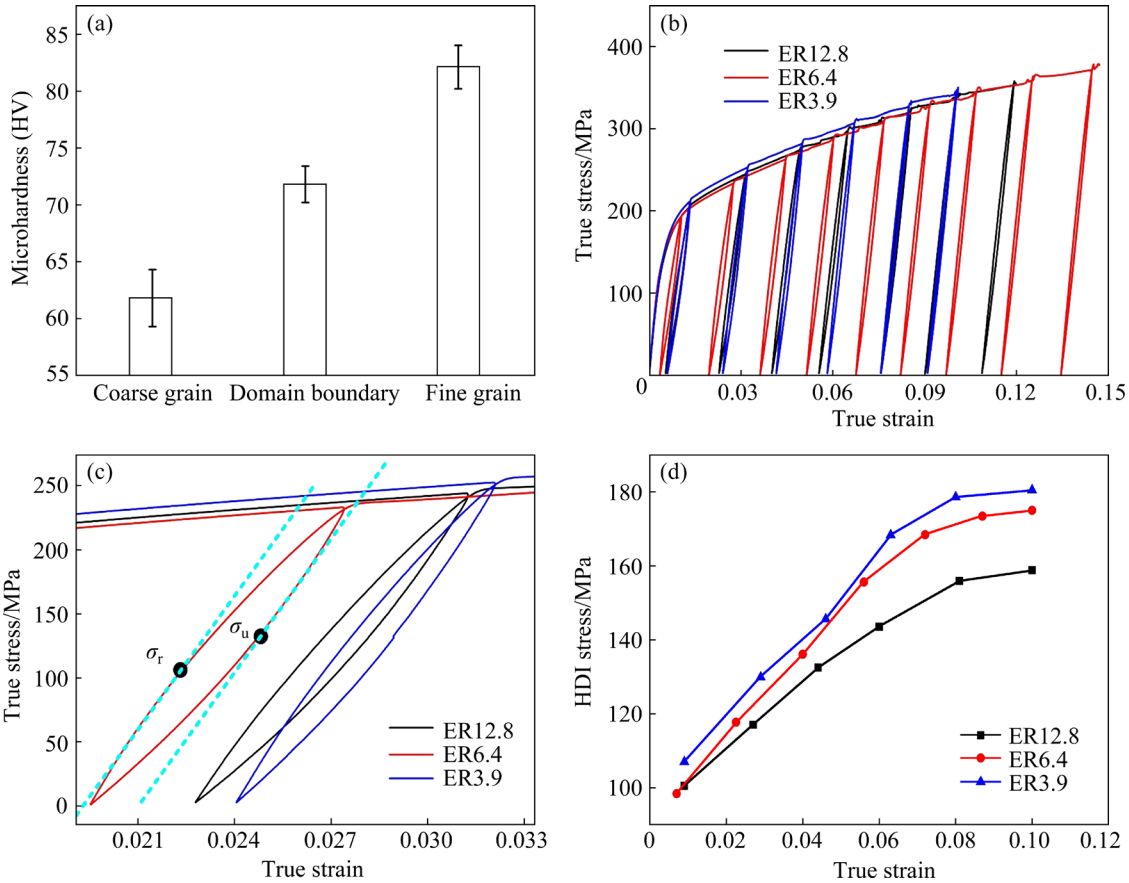

Fig. 7 Microhardness of ER3.9 sample (a); LUR tensile curves of ER12.8, ER6.4 and ER3.9 samples (b); Partially amplified hysteresis loops of three samples (c); Calculated HDI stress (d) based on Fig. 7(b)

presented in Fig. 7(c). Figure 7(d) shows the development of HDI stress in the three samples as the strain increases. It can be seen that their HDI stress increases almost linearly before reaching a strain of 6%. Thereafter, the HDI stress gradually levels off, which is related to the saturated GNDs and the interaction between the GNDs and mobile dislocations, impeding the pile-up of GNDs towards domain boundary. Besides, the HDI stress of the ER3.9 sample is higher than that of the ER6.4 and ER12.8 samples during deformation. This suggests that the dual-heterostructure of grain size and precipitates can produce a higher HDI strengthening and hardening effect, which contributes to the extra strengthening and strain.

However, a large number of banded $Mg_{17}Al_{12}$ precipitates in the fine-grained layers of the ER3.9 sample become the crack sources and greatly deteriorate the ductility (Fig. 4(i)). Combined with the tensile properties of the three samples, it is concluded that the optimal HDI strengthening and hardening effect and higher SF for basal slip should not be the dominant role in improving the mechanical properties of the ER3.9 sample due to the existence of profuse banded precipitates. For the ER6.4 sample, it has an area proportion of 12.7% in the fine-grained layers and decreased banded precipitates. Figures 8(a, b) indicate that a large number of dislocations in the ER6.4 sample are pinned by precipitates at strain of 6.8%. The high-resolution TEM images in Figs. 8(d, e) demonstrate that a misfit strain field exists between precipitates and dislocations, further confirming this pinning effect. It should be pointed that unlike bowed dislocation lines that intersect precipitates (marked by yellow arrows), these straight dislocations embed in precipitates (marked by blue arrows), which may be the consequence of dislocation-assisted nucleation rather than the pinning dislocation by precipitates [23]. In addition, Fig. 8(c) shows another lower magnification bright-field image in Fig. 8(a), which exhibits various morphologies of precipitates, such as spherical, rod-like and lamellar precipitates. The average size of these precipitates is 83.7 nm (Fig. 8(f)). It has been reported that fine precipitates not only hinder the dislocation movement to enhance the strength based on Orowan mechanism, but also relieve the stress concentration to maintain ductility [24,34,35]. Therefore, the synergistic effects of fine precipitates

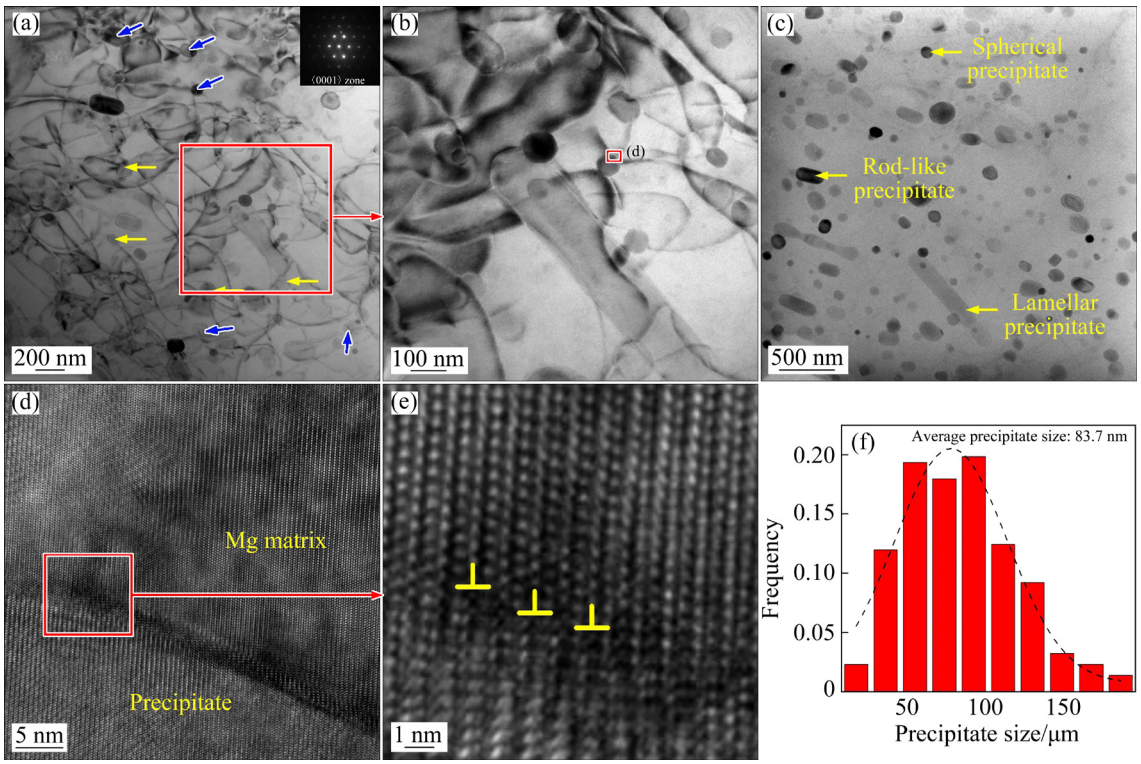

Fig. 8 Bright-field TEM image near ⟨0001⟩ of ER6.4 sample at strain of 6.8% under two-beam condition (a, b); Bright-field image to reflect distribution of precipitates (c); High-resolution TEM images of pinning dislocations by precipitates (d, e); Distribution of precipitates size (f)

and heterogeneous deformation of the ER6.4 sample achieve a balance of precipitate strengthening and hardening as well as HDI strengthening and hardening, improving its strength and ductility simultaneously.

4.2 Fracture behavior of dual-heterogeneous structure

In order to evaluate the effect of banded precipitates on the mechanical properties, it is necessary to study the fracture mechanism of the ER3.9 sample, which is pursued via the investigation of tensile fracture. Figure 9(a) presents the SEM images on the ED−ND plane of the ER3.9 sample after fracture. It can be seen that the cracks initiate on banded $Mg_{17}Al_{12}$ precipitates in fine-grained layers and are nearly perpendicular to the tensile direction near the fracture (Fig. 9(b)). Meanwhile, the propagation of cracks terminates in the coarse-grained layers, which indicates that the coarse-grained layers can effectively blunt propagating crack tips and constrain their growth (Fig. 9(c)).

According to the observed results above, a descriptive model of tensile fracture in the dual-heterogeneous AZ91 alloy is proposed. The tensile fracture process of the ER3.9 sample can be illustrated by the following three stages shown in Fig. 9(e). At Stage I, the plastic deformation occurs preferentially in the coarse-grained layers when the tensile stress along the ED achieves the yield point of coarse grains. As the stress continues to increase and reaches the yield point of fine grains, the crack sources first appear on the banded precipitates in the fine-grained layers, while a few voids occur in the coarse-grained layers due to the coarse precipitates (Fig. 9(d)). At Stage II, the cracks grow from the banded precipitates, similar to the crack nucleation sites of the Mg−11Y−5Gd−2Zn−0.5Zr alloy [36]. As tensile stress further increases, the

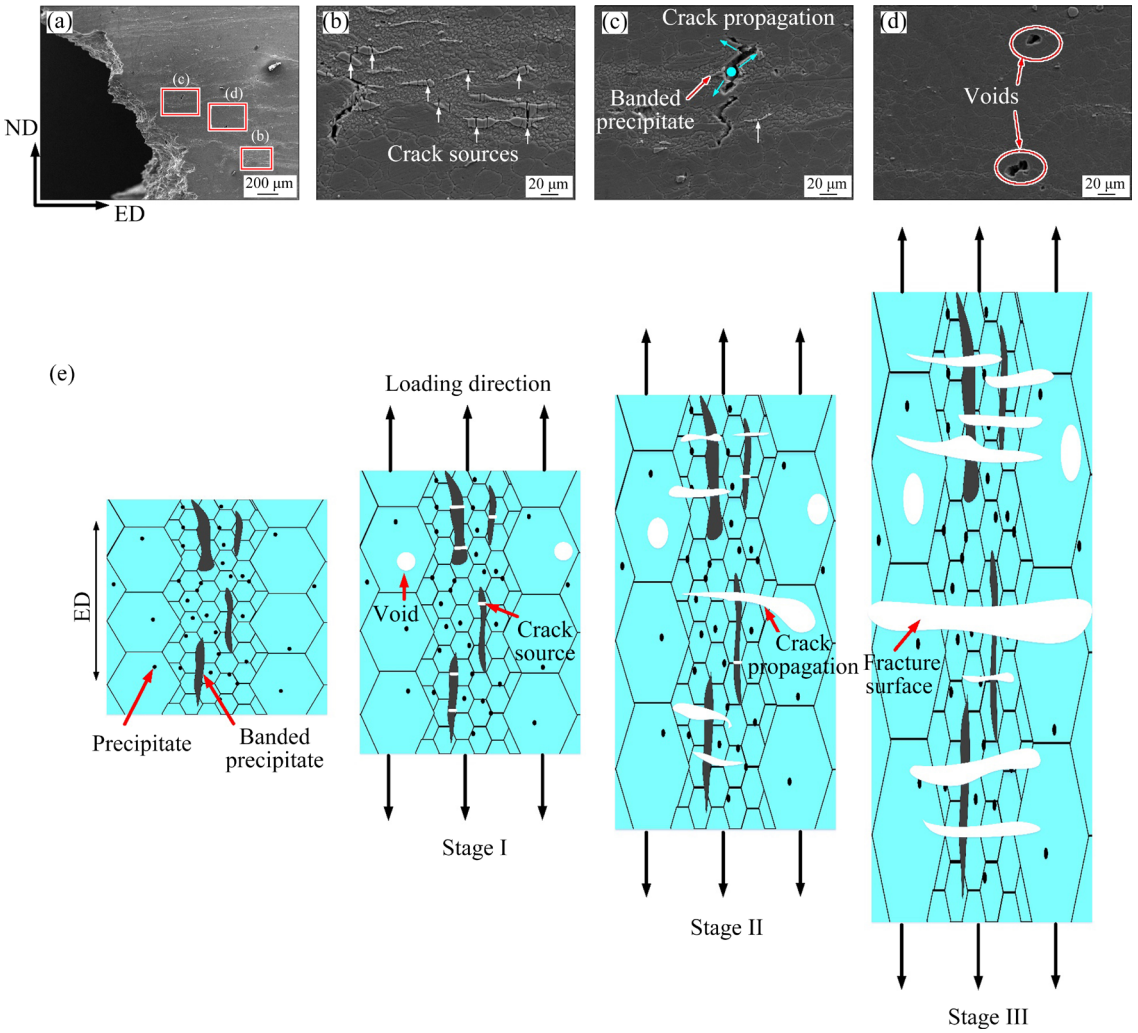

Fig. 9 SEM images on ED−ND plane near fracture (a−d); Schematic of tensile deformation and fracture mechanism of ER3.9 sample in uniaxial tension along ED (e)

cracks propagate almost perpendicular to the load axis, exhibiting transgranular and intergranular cracking, which is related to the local slip and twin behavior [37]. And also, the voids in the coarse-grained layers also induce stress concentration, resulting in their growth and extension along the tensile stress direction [38]. However, the coarse grains bridge and blunt the cracks, efficiently hampering the propagation of cracks. At Stage III, failure fracture occurs when the cracks link, and the coarse-grained layers can no longer maintain the applied load. Despite the fact that the coarse-grained layers limit the growth and propagation of cracks in the fine-grained layers, the presence of more crack sources accelerates the fracture of the sample. Therefore, the reduced banded precipitates in the ER6.4 sample exhibit a promising advantage in the ductile-phase toughening mechanism.

The present work provides valuable insights into the design of a dual-heterogeneous structure that can effectively resist fracture while enhancing ductility. Utilizing this design method, the single materials with dual-heterogeneous structure can acquire unique combinations of strength and ductility. It has been suggested that the heterostructured materials with an appropriate proportion of hard and soft regions are capable of achieving the optimal HDI strengthening and hardening effect, which greatly affects their strength and ductility [10]. For instance, the fine-grained layers with high density precipitates in AZ91 alloy possessed an area proportion of 26.8%, which maximized HDI strengthening and hardening [26]. MA et al [39] found that the nanostructured Cu−10Zn layer, accounting for a volume fraction of 22%, exhibited excellent combination of strength and ductility. Related researches also include pure Ti [6], and dual-phase steels [40]. Therefore, in order to optimize the mechanical properties, further work is warranted to consider two critical factors: (1) the area proportion and distribution of the coarse-grained layers and (2) the regulation of banded precipitates.

5 Conclusions

(1) The ER3.9 and ER6.4 samples present a dual-heterostructure of grain size and precipitates, especially the ER3.9 sample. However, a large number of banded precipitates are distributed in the fine-grained layers of the ER3.9 sample, in addition to fine-dispersed precipitates.

(2) The ER6.4 sample presents an excellent combination of strength and ductility due to the synergistic effect of precipitate and HDI stress. The LUR tests indicate that the ER3.9 sample has the highest HDI stress, but the banded precipitates play a dominant role in deteriorating its ductility although the HDI hardening and high SF for basal slip contribute to the improvement of ductility.

(3) The coarse-grained layers effectively limit the growth and propagation of cracks in the fine-grained layers and delay the failure fracture of the sample, exhibiting a ductile-phase toughening mechanism.

Acknowledgments

This work was supported by the National Natural Science Foundation of China (No. 52071035), and Guangdong Major Project of Basic and Applied Basic Research, China (No. 2020B0301030006).

References

[1] XIE Jin-shu, ZHANG Jing-huai, YOU Zi-hao, LIU Shu-juan, GUAN Kai, WU Rui-zhi, WANG Jun, FENG Jing. Towards developing Mg alloys with simultaneously improved strength and corrosion resistance via RE alloying [J]. Journal of Magnesium and Alloys, 2021, 9(1): 41−56.

[2] MA Ying-zhong, WANG De-xin, LI Hong-xiang, YANG Chang-lin, YUAN Fu-song, ZHANG Ji-shan. Microstructure, mechanical properties and corrosion behavior of quaternary Mg−1Zn−0.2Ca−*x*Ag alloy wires applied as degradable anastomotic nails [J]. Transactions of Nonferrous Metals Society of China, 2021, 31(1): 111−124.

[3] WEI Xiao-xiao, JIN Li, WANG Feng-hua, LI Jing, YE Nan, ZHANG Zhen-yan, DONG Jie. High strength and ductility Mg−8Gd−3Y−0.5Zr alloy with bimodal structure and nano-precipitates [J]. Journal of Materials Science & Technology, 2020, 44: 19−23.

[4] YANG Yan, XIONG Xiao-ming, CHEN Jing, PENG Xiao-dong, CHEN Dao-lun, PAN Fu-sheng. Research advances in magnesium and magnesium alloys worldwide in 2020 [J]. Journal of Magnesium and Alloys, 2021, 9(3): 705−747.

[5] WANG Bo-ning, WANG Feng, WANG Zhi, LIU Zheng, MAO Ping-li. Fabrication of fine-grained, high strength and toughness Mg alloy by extrusion-shearing process [J]. Transactions of Nonferrous Metals Society of China, 2021, 31(3): 666−678.

[6] WU Xiao-lei, YANG Mu-xin, YUAN Fu-ping, WU Gui-lin, WEI Yu-jie, HUANG Xiao-xu, ZHU Yun-tian. Heterogeneous lamella structure unites ultrafine-grain

strength with coarse-grain ductility [J]. Proceedings of the National Academy of Sciences, 2015, 112(47): 14501−14505.

[7] ZHANG Ling, CHEN Zhen, WANG Yu-hui, MA Guo-qiang, HUANG Tian-lin, WU Gui-lin, JENSEN D J. Fabricating interstitial-free steel with simultaneous high strength and good ductility with homogeneous layer and lamella structure [J]. Scripta Materialia, 2017, 141: 111−114.

[8] LIANG Fei, LUO Xue-mei, ZHANG Guang-ping. Interface-coupling-dependent mechanical behaviors of sandwich-structured Ni/Cu/Ni composites [J]. Materials Science and Engineering A, 2019, 743: 436−444.

[9] MA Xiao-long, HUANG Chong-xiang, MOERING J, RUPPERT M, HOPPEL H W, GOKEN M, NARAYAN J, ZHU Yun-tian. Mechanical properties of copper/bronze laminates: Role of interfaces [J]. Acta Materialia, 2016, 116: 43−52.

[10] WU Xiao-lei, ZHU Yun-tian. Heterogeneous materials: A new class of materials with unprecedented mechanical properties [J]. Materials Research Letters, 2017, 5(8): 527−532.

[11] WANG Yan-fei, YANG Mu-xin, MA Xiao-long, WANG Ming-sai, YIN Kun, HUANG Ai-hui, HUANG Chong-xiang. Improved back stress and synergetic strain hardening in coarse-grain/nanostructure laminates [J]. Materials Science and Engineering A, 2018, 727: 113−118.

[12] ZHU Yun-tian, WU Xiao-lei. Perspective on hetero-deformation induced (HDI) hardening and back stress [J]. Materials Research Letters, 2019, 7(10): 393−398.

[13] LIU Shuai-shuai, LIU Han, CHEN Xiang, HUANG Guang-sheng, ZOU Qin, TANG Ai-tao, JIANG Bin, ZHU Yun-tian, PAN Fu-sheng. Effect of texture on deformation behavior of heterogeneous Mg−13Gd alloy with strength-ductility synergy [J]. Journal of Materials Science & Technology, 2022, 113: 271−286.

[14] FANG Xiao-tian, LI Zhong-kai, RUIZ M, MA Xiao-long, WANG Hui-yuan, ZHU Yong, SCHOELL R, ZHENG Ce, KAOUMI D, ZHU Yun-tian. Achieving high hetero-deformation induced (HDI) strengthening and hardening in brass by dual heterostructures [J]. Journal of Materials Science & Technology, 2022, 98: 244−247.

[15] HUANG Jia-xi, LIU Yong-ning, XU Tao, CHEN Xue-fei, LAI Qing-quan, XIAO Lai-rong, PAN Zhi-yi, GAO Bo, ZHOU Hao, ZHU Yun-tian. Dual-phase hetero-structured strategy to improve ductility of a low carbon martensitic steel [J]. Materials Science and Engineering A, 2022, 834: 142584.

[16] HAN Ting-zhuang, HUANG Guang-sheng, DENG Qian-yuan, WANG Guan-gang, JIANG Bin, TANG Ai-tao, ZHU Yun-tian, PAN Fu-sheng. Grain refining and mechanical properties of AZ31 alloy processed by accumulated extrusion bonding [J]. Journal of Alloys and Compounds, 2018, 745: 599−608.

[17] JUNG J, PARK S H, YU H, KIM Y M, LEE Y K, YOU B S. Improved mechanical properties of Mg−7.6Al−0.4Zn alloy through aging prior to extrusion [J]. Scripta Materialia, 2014, 93(15): 8−11.

[18] CORBY C, CACERES C H, LUKAC P. Serrated flow in magnesium alloy AZ91 [J]. Materials Science and Engineering A, 2004, 387/288/389: 22−24.

[19] YUAN Yu-chun, MA Ai-bin, JIANG Jing-hua, LU Fu-min, JIAN Wei-wei, SONG Dan, ZHU Yun-tian. Optimizing the strength and ductility of AZ91 Mg alloy by ECAP and subsequent aging [J]. Materials Science and Engineering A, 2013, 588: 329−334.

[20] SUN Jia-peng, XU Bing-qian, YANG Zhen-quan, ZHUO Xiao-ru, HAN Jing, WU Yu-na, SONG Dan, LIU Huan, JIANG Jing-hua, MA Ai-bin. Developing an industrial-scale ECAP Mg−Al−Zn alloy with multi-heterostructure for synchronously high strength and good ductility [J]. Materials Characterization, 2020, 164: 110341.

[21] SUN Jia-peng, YANG Zhen-quan, HAN Jing, LIU Huan, SONG Dan, JIANG Jing-hua, MA Ai-bin. High strength and ductility AZ91 magnesium alloy with multi-heterogenous microstructures prepared by high-temperature ECAP and short-time aging [J]. Materials Science and Engineering A, 2018, 734: 485−490.

[22] YANG Zhen-quan, MA Ai-bin, LIU Huan, SONG Dan, WU Yu-na, YUAN Yu-chun, JIANG Jing-hua, SUN Jia-peng. Managing strength and ductility in AZ91 magnesium alloy through ECAP combined with prior and post aging treatment [J]. Materials Characterization, 2019, 152: 213−222.

[23] ROBSON J D, HENRY D T, DAVIS B. Particle effects on recrystallization in magnesium–manganese alloys: Particle-stimulated nucleation [J]. Acta Materialia, 2009, 57(9): 2739−2747.

[24] LIU Shuai-shuai, WANG Wei-zhang, CHEN Xiang, HUANG Guang-sheng, LIU Han, TANG Ai-tao, JIANG Bin, PAN Fu-sheng. Enhanced strength and ductility AZ91 alloy with heterogeneous lamella structure prepared by pre-aging and low-temperature extrusion [J]. Materials Science and Engineering A, 2021, 812: 141094.

[25] LIN Xiao-ping, KUO Yang, WANG Lin, YE Jie, ZHANG Chong, WANG Li, GUO Kun-yu. Refinement and strengthening mechanism of Mg−Zn−Cu−Zr−Ca alloy solidified under extremely high pressure [J]. Transactions of Nonferrous Metals Society of China, 2021, 31(6): 1587−1598.

[26] LIU Shuai-shuai, ZHANG Bao-xuan, LIU Han, HUANG Guang-sheng, ZOU Qin, TANG Ai-tao, JIANG Bin, PAN Fu-sheng. Achieving strength-ductility synergy of AZ91 extruded sheet by balancing dual-heterostructure of grain size and precipitates [J]. Materials Science and Engineering A, 2021, 827: 141989.

[27] YIN Dong-di, BOEHLERT C J, HUANG Guang-hao, ZHOU Hao, ZHENG Jiang, WANG Qu-dong. Tension−compression asymmetry and the underlying slip/twinning activity in extruded Mg−Y sheets [J]. International Journal of Plasticity, 2021, 136: 102878.

[28] NI Ren-jie, YIN Dong-di, ZHOU Hao, ZHENG Jiang, WANG Qu-dong. Investigation on slip activity and plastic heterogeneity of aged Mg−10Y sheets during compression [J]. Metallurgical and Materials Transactions A, 2021. Doi: 10.1007/s11661-021-06523-y.

[29] FANG Xiao-tian, ZHENG Ce, MA Xiao-long, KAOUMI D, LI Yu-sheng, ZHU Yun-tian. Effect of heterostructure and hetero-deformation induced hardening on the strength and ductility of brass [J]. Acta Materialia, 2020, 186: 644−655.

[30] LIU Yan-fang, CAO Yang, MAO Qing-zhong, ZHOU Hao, ZHAO Yong-hao, JIANG Wei, LIU Ying, WANG Jing-tao, YOU Ze-sheng, ZHU Yun-tian. Critical microstructures and defects in heterostructured materials and their effects on mechanical properties [J]. Acta Materialia, 2020, 189: 129−144.

[31] YANG Mu-xin, PAN Yue, YUAN Fu-ping, ZHU Yun-tian, WU Xiao-lei. Back stress strengthening and strain hardening in gradient structure [J]. Materials Research Letters, 2016, 4(3): 145−151.

[32] HE Jin-yan, MA Yan, YAN Ding-shun, JIAO Si-hai, YUAN Fu-ping, WU Xiao-lei. Improving ductility by increasing fraction of interfacial zone in low C steel/304 SS laminates [J]. Materials Science and Engineering A, 2018, 726: 288−297.

[33] REN Ping, CHEN Xing-pin, CAO Zhao-xi, MEI Lin, LI Wen-jia, CAO Wen-quan, LIU Qing. Synergistic strengthening effect induced ultrahigh yield strength in lightweight Fe−30Mn−11Al−1.2C steel [J]. Materials Science and Engineering A, 2019, 752: 160−166.

[34] CHEN Xing-pin, LI Shun, MEI Lin, REN Ping, LIU Qing. Excellent combination of strength and ductility of Al−1.2Mn alloy with multi-scale lamellar structure [J]. Materials Science and Engineering A, 2018, 729: 458−465.

[35] LI Zhi-feng, DONG Jie, ZENG Xiao-qing, LU Chen, DING Weng-jiang. Influence of Mg17Al12 intermetallic compounds on the hot extruded microstructures and mechanical properties of Mg−9Al−1Zn alloy [J]. Materials Science and Engineering A, 2007, 466: 134−139.

[36] YIN Dong-di, WANG Qu-dong, BOEHLERT C J, MISHRA R K, CHAKKEDATH A. In-situ study of the tensile deformation and fracture modes in peak-aged cast Mg−11Y−5Gd−2Zn−0.5Zr (Weight Percent) [J]. Metallurgical and Materials Transactions A, 2016, 47(12): 6438−6452.

[37] DENG Y C, HUANG Z J, LI T J, YIN Dong-di, ZHENG Jiang. Quantitative investigation on the slip/twinning activity and cracking behavior during low-cycle fatigue of an extruded Mg−3Y sheet [J]. Metallurgical and Materials Transactions A, 2021, 52(1): 332−349.

[38] NASERI M, REIHANIAN M, BORHANI E. A new strategy to simultaneous increase in the strength and ductility of AA2024 alloy via accumulative roll bonding (ARB) [J]. Materials Science and Engineering A, 2016, 656: 12−20.

[39] MA Xiao-long, HUANG Chong-xiang, XU Wei-zong, ZHOU Hao, WU Xiao-lei, ZHU Yun-tian. Strain hardening and ductility in a coarse-grain/nanostructure laminate material [J]. Scripta Materialia, 2015, 103: 57−60.

[40] CALCAGNOTTO M, ADACHI Y, PONGE D. Deformation and fracture mechanisms in fine- and ultrafine-grained ferrite/martensite dual-phase steels and the effect of aging [J]. Acta Materialia, 2011, 59: 658−670.

双重异质结构对 AZ91 挤压板力学性能的影响

刘帅帅[1,2]，杨邦鹏[1,2]，黄光胜[1,2]，陈先华[1,2]，汤爱涛[1,2]，蒋 斌[1,2]，郑开宏[3]，潘复生[1,2]

1. 重庆大学 材料科学与工程学院 机械传动国家重点实验室，重庆 400044；
2. 重庆大学 国家镁合金工程研究中心，重庆 400044；
3. 广东省科学院 新材料研究所，广州 510650

摘 要：研究晶粒尺寸和析出相的双重异质结构对小挤压比制备的 AZ91 挤压板材力学性能的影响。与挤压比(ER)为12.8的样品(即ER12.8样品)相比，ER3.9和ER6.4样品呈现明显的粗细晶粒层和异质分布的细小弥散的析出相。此外，在 ER3.9 样品的细晶层中还观察到大量带状析出相。由于异质变形诱导(HDI)力和析出相的平衡，ER6.4 样品呈现良好的强度和塑性结合。尽管 ER3.9 样品表现出最高的 HDI 力和基面滑移施密特因子，改善了塑性，但更多的带状析出相对恶化其力学性能仍起主导作用。

关键词：AZ91 合金；双重异质结构；析出相；力学性能；异质变形诱导(HDI)力

(Edited by Bing YANG)